NASA TM X-20

NASA TM X-20

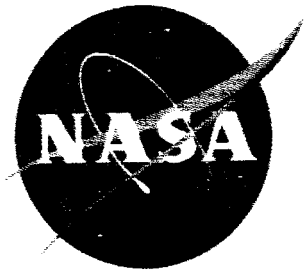

TECHNICAL MEMORANDUM

X - 20

SOME MEASUREMENTS OF THE DYNAMIC AND STATIC STABILITY OF TWO BLUNT-NOSED, LOW-FINENESS-RATIO BODIES OF REVOLUTION IN FREE FLIGHT AT M = 4

By Barbara J. Short and Simon C. Sommer

Ames Research Center
Moffett Field, Calif.

NATIONAL AERONAUTICS AND SPACE ADMINISTRATION
WASHINGTON
October 1959

X-64

NATIONAL AERONAUTICS AND SPACE ADMINISTRATION

TECHNICAL MEMORANDUM X-20

SOME MEASUREMENTS OF THE DYNAMIC AND STATIC STABILITY OF TWO BLUNT-NOSED, LOW-FINENESS-RATIO BODIES OF REVOLUTION IN FREE FLIGHT AT M = 4*

By Barbara J. Short and Simon C. Sommer

SUMMARY

Measurements have been made at a Mach number near 4 of the dynamic and static stability and drag of two blunt-nosed, low-fineness-ratio bodies of revolution in free flight. One model had a parabolic forebody and the other had a nearly flat front face.

The experimentally determined dynamic stability was found to be a function of angle of attack. The flat-faced model was dynamically unstable throughout the angle-of-attack range covered, 4° to 16°. The parabolic body was found to be dynamically stable throughout most of the angle-of-attack range covered by the tests but was unstable at the lowest angle, 4°, and neutrally stable at the highest angle, 27°. Modified Newtonian impact theory generally predicted the magnitude of the dynamic stability parameter but not the variation with angle of attack.

INTRODUCTION

Investigations of the oscillatory behavior of ballistic vehicles entering the earth's atmosphere at high speeds (refs. 1 and 2) have shown that the restraint of the amplitude of their oscillations is primarily due to the rapid increase of atmospheric density. In fact, during the early phase of the descent to the altitude at which maximum dynamic pressure is experienced, vehicles which would be dynamically unstable in flight at constant altitude nevertheless will undergo oscillations which are convergent. For such vehicles, the altitude at which divergence will occur and the magnitude of the divergence have been shown to be a function of the dynamic instability as well as the static flight trajectory of the vehicle (ref. 3).

*Title, Unclassified

Vehicles being considered for re-entry flight are of the high-drag, low-fineness-ratio type; consequently, the dynamic stability of such shapes is of interest. A program was therefore initiated in several facilities of the Ames Research Center to measure the stability and drag characteristics of two low-fineness-ratio, high-drag configurations through the Mach number range from subsonic to moderate supersonic speeds. The two configurations chosen were a paraboloid and a nearly flat-faced body, which represent two different design approaches for ballistic vehicles. The investigation at a nominal Mach number of 4 was conducted in the Ames supersonic free-flight wind tunnel, and the results are presented herein.

SYMBOLS

A	frontal area, sq ft
C_D	drag coefficient, $\frac{\text{drag}}{q_\infty A}$, dimensionless
C_{L_α}	lift-curve slope, per radian
C_m	pitching-moment coefficient, $\frac{\text{pitching moment}}{q_\infty A d}$, dimensionless
C_{m_α}	pitching-moment-curve slope, per radian
$C_{m_q}+C_{m_{\dot\alpha}}$	damping-in-pitch derivative, dimensionless $\frac{\partial C_m}{\partial[q(d/V)]} + \frac{\partial C_m}{\partial[\dot\alpha(d/V)]}$,
C_{N_α}	normal-force-curve slope, $C_{L_\alpha} + C_D$, dimensionless
d	maximum body diameter, ft
I_y	transverse moment of inertia, mo^2, slug-ft^2
$K_{1,2,3}$	constants in equation (2), deg
l	length of model forebody, ft
m	mass of model, slugs
M	Mach number
p	roll parameter, $\frac{\text{roll rate}}{\text{velocity}}$, radians/ft

q	angular pitching velocity, radians/sec
q_∞	free-stream dynamic pressure, lb/sq ft
r	radius of base of model forebody, ft
V	velocity along flight path, ft/sec
x	distance along flight path or coordinate along body axis, ft
y	coordinate normal to body axis, ft
α	angle of attack (in the vertical plane), deg
α_m	peak amplitude of oscillation in combined pitch and yaw, deg
β	angle of sideslip (in the horizontal plane), deg
$\eta_{1,2}$	damping exponents in equation (2), ft^{-1}
λ	wave length of pitching oscillation, ft/cycle
ρ_∞	free-stream air density, slugs/cu ft
σ	transverse radius of gyration, ft
$\omega_{1,2}$	rates of rotation of vectors which generate the model pitching motion, radians/ft
ξ	dynamic stability parameter, $C_D - C_{L_\alpha} + (C_{m_q}+C_{m_{\dot{\alpha}}})(d/\sigma)^2$, dimensionless

Superscript

$(\dot{})$	first derivative with respect to time

DESCRIPTION OF TESTS

The two blunt bodies shown in figure 1 were tested in free flight through still air at atmospheric pressure to determine their dynamic and static stability and drag. The models were launched from a 1.75-inch-diameter, smooth-bore gun to give a velocity in the test section of about 4600 feet per second, corresponding to a nominal Mach number of 4 and a nominal Reynolds number of 3×10^6 based on free-stream conditions and

model diameter. Angle-of-attack and time-distance histories were recorded in the test section at nine shadowgraph stations and with a chronograph. The dynamic and static stability were obtained from the angle-of-attack histories which were analyzed to define the growth or decay of the pitching motion and the wave length of oscillation. Total drag coefficients were computed from deceleration data.

Models and Launching Technique

One model had a parabolic forebody, and the other model had a nearly flat front face. The models were designed to have a given center-of-gravity location and a given value of $(d/\sigma)^2$ to enable a direct comparison of results from the various facilities of the Ames Research Center (refs. 4, 5, and 6). In order to scale the models properly, they were made bimetallic. The forebodies of both model shapes were machined from SAE 4130 steel. The afterbody of the parabolic model was machined from AZ80A magnesium, and the afterbody of the flat-faced model was machined from 7075-T6 aluminum. The notch in the afterbody and the spike on the back of the model, shown in figure 1, were aids used in measuring the angular orientation of the model from the shadowgraphs. All models were polished to a maximum surface roughness of about 20 microinches.

The sabot used for launching the models is shown in figure 2 with the paraboloid. The screw threads on the afterbodies of the models (fig. 1) were used to hold the models in the sabots. As can be seen in figure 2, the nylon sabots were made in two pieces with a canted front face. The split sabot allowed for model and sabot separation; whereas, the canted front face induced angle of attack to the model. For each model launched, the sabot cant angle was chosen to give the desired peak amplitude of oscillation. The peak amplitude was generally from 2 to 3 times the angle of cant of the sabot, although one launching produced a peak angle of attack five times the canted angle. The sabots were canted with angles of from 2° to 6°, which induced peak amplitudes of oscillation to the models of from 4° to 27°.

Figure 3 shows typical shadowgraphs taken in these tests, one for each model. In both shadowgraphs the models are near zero angle of attack.

STABILITY DATA REDUCTION

The growth or decay of the motion of a vehicle in flight is a measure of the dynamic stability. The frequency of oscillation is a measure of the static stability. It was shown by Allen in reference 2 that a convenient parameter which describes the dynamic stability of a vehicle entering the atmosphere is of the form,

$$\xi = C_D - C_{I_\alpha} + (C_{m_q}+C_{m_{\dot{\alpha}}})(d/\sigma)^2 \qquad (1)$$

In reference 7 it was shown that this same parameter describes the dynamic stability of a vehicle flying at constant altitude. In reference 7 the equation of pitching motion was developed for unconstrained flight with the assumptions of a nonspinning body of revolution at zero angle of trim with linear aerodynamic moments. Inspection of the motions of the present test models showed that these assumptions would not allow analytical representation of the motions with sufficient accuracy to define the damping. In particular, the motions, all of which are shown plotted in figure 4, indicated that the models were flying with small trim angle and small rolling velocity. Examination of the motions in the α - β plane shows distorted ellipses which precess due to model spin. In order to prove that the models were indeed spinning, four pegs were installed in the afterbody of one model. The amount of spin measured was compatible with the observed precession. (Although the models were launched from a smooth-bore gun, the sabots evidently imparted a small amount of spin to the models.) Analysis of the data also showed the presence of small angles of trim. Although the models were axially symmetric, they were bimetallic and slight misalinement in the construction could cause the center of gravity to be shifted off the axis of rotation. This shift, in turn, would cause the model to trim in flight.

An examination of the typical angle-distance histories in figures 4(i) and 4(j) shows the motion to be convergent in one plane (α plane, fig. 4(j)) and divergent in the other (β plane, fig. 4(j)). Since the motions are inertially coupled, the analysis by individual planes separately leads to an erroneous result.

In order to determine the parameter ξ from the data of the present tests, therefore, the tricyclic theory of pitching and yawing motion was used. This theory was developed by Nicolaides in reference 8 and includes the effects of trim and spin on the model motions. The solution of the differential equation of motion as given by Nicolaides is rewritten here in the nomenclature of this report,

$$\beta + i\alpha = K_1 e^{(\eta_1+i\omega_1)x} + K_2 e^{(\eta_2-i\omega_2)x} + K_3 e^{ipx} \qquad (2)$$

where

$$\eta_1 + \eta_2 = \frac{\rho_\infty A}{2m}\xi \qquad (3)$$

and

$$\frac{2\pi}{\sqrt{\omega_1\omega_2}} = \lambda \qquad (4)$$

Equation (2) was fitted to the measurements of α and β of each flight by the method of differential corrections as described by Shinbrot in reference 9. The curves shown in figure 4 were obtained by use of equation (2). It can be seen that although the motions are widely varied, equation (2) fitted to the data of each flight does represent the actual free-flight motions of these models.

The dynamic stability parameter, ξ, was calculated from the constants η_1 and η_2 by use of the relationship shown in equation (3). The static stability derivative was computed from the wave length of oscillation (eq. (4)) by means of the relation,

$$C_{m_\alpha} = - \frac{8\pi^2 I_y}{\lambda^2 \rho_\infty A d} \tag{5}$$

which is developed in reference 7.

The scatter in the measurements of the angles of pitch and yaw from the shadowgraphs can be considered as a measure of the accuracy of the dynamic stability parameter, ξ. A probable error of 0.03° in the angle measurements was determined statistically from many readings by several observers. If the errors in the angle-of-attack readings were oriented in the worst possible arrangement, this would result in error of ξ of ± 0.4 at the low angle of attack and ± 0.1 at the high angle of attack.

RESULTS AND DISCUSSION

Dynamic Stability

The results of the dynamic stability tests are presented in figure 5, where the dynamic stability parameter, ξ, is plotted as a function of amplitude of oscillation, α_m. The parameter ξ is positive when the model motion is divergent (dynamic instability) and is negative when the model motion is convergent (dynamic stability). Values of $\xi = 0$ represent neutral stability. These values of ξ presented in the figure were calculated with the assumption of a linear system over the amplitude range covered by any one test. The data of reference 4, which cover an angle-of-attack range up to 12° in the same Mach number range as the present tests, show that the nonlinearities in the static aerodynamic moments on these two body shapes are small. It can be seen in figure 5, however, that there is a considerable dependence of damping on angle of attack. In each of the present test flights, the model oscillated through an angle-of-attack range from near 0° to the peak amplitude at which ξ is plotted. The value of ξ measured for that amplitude range is therefore the dynamic stability parameter of an equivalent linear system whose oscillation amplitude over the same range would decay in the same way as that experienced by the model.

It can be seen in figure 5 that the flat-faced model was dynamically unstable throughout the angle-of-attack range covered by the tests. The greatest instability occurred when the model oscillated up to 8° amplitude. The parabolic model was dynamically stable throughout most of the angle range covered by the tests. This model was unstable, however, at the lowest amplitude tested, 4°, and neutrally stable at the highest angle, 27°.

The filled symbol on the curve for the flat-faced model at $\alpha_m = 5^\circ$ is the result of one confirming test made in the new 203-foot long pressurized ballistic range. This facility became available after the present investigation was almost completed. The data from this flight were incomplete because only 14 of the 24 measuring stations were available at the time of testing. This left a gap of 98 feet in the record of the model motion. The length of flight path, however, was eight times the length of flight path in the wind tunnel so that considerably more cycles of oscillation occurred. The result obtained is included in figure 5 and shows excellent agreement of the data from the two facilities.

Included in figure 5 are two values of ξ, one for each model, obtained from the data of the Ames 8- by 7-foot wind tunnel at a Mach number of 3.5 (ref. 5). These data points were obtained from forced oscillations of limited amplitude (1.5°) about zero angle of attack. The data obtained in this wind tunnel show that when the models were oscillated 1.5° about angles other than zero, the dynamic stability of the paraboloid changed very little, whereas there was a sharp decrease of instability with small changes of angle of attack from zero for the flat-faced model. The two points shown in figure 5 were the only wind-tunnel data at conditions which approximated those of the present investigation, that is, models oscillating through an angle range from near zero to the angle at which ξ is plotted. The conclusion that there is a discrepancy in the data from the two facilities for the flat-faced model may not be warranted because the lowest amplitude obtained in the present tests was about 4°. It is unknown what the value of ξ would be as measured in free flight at angles of the order of 1° or 2°.

Comparison between values of ξ obtained from the modified Newtonian impact theory[1] and experiment is also shown in figure 5. For the conditions of these tests, the theory did not indicate any variation of ξ with angle of attack.

The damping-in-pitch derivative, $C_{m_q} + C_{m_{\dot{\alpha}}}$, expresses the dynamic stability of a model at constant velocity when the model is not free to plunge, as, for example, in wind-tunnel tests. This derivative was formed by combining the values of ξ and C_D from the data of the present tests with values of C_{N_α} obtained from wind-tunnel measurements. These results are shown in figure 6. It is important to note that although the flat-faced

[1]Newtonian impact theory was modified by replacing the coefficient 2 by the stagnation-pressure coefficient behind a normal shock wave.

model is dynamically unstable ($\xi > 0$), the damping-in-pitch derivative is stabilizing ($C_{m_q} + C_{m_{\dot{\alpha}}} < 0$) except near 8° amplitude. For the parabolic model, the damping-in-pitch derivative is negative throughout most of the angle range, whereas, as seen in figure 5, this model is unstable near 4° and neutrally stable near 27° amplitude. It is apparent that so-called "stable" values of the damping-in-pitch derivative ($C_{m_q} + C_{m_{\dot{\alpha}}} < 0$) do not in themselves indicate convergent oscillations for a vehicle in free flight. It can be seen from equation (1) that the combination of C_D and C_{L_α} can overshadow a stabilizing damping-in-pitch derivative to produce a divergent motion.

Also shown in figure 6 are values of the damping-in-pitch derivatives obtained from modified Newtonian impact theory.

Static Stability

Moment-curve slopes, as a measure of the static stability, are presented in figure 7 where C_{m_α} is plotted as a function of Mach number. The data from the present tests are shown by the circle symbols and are compared with data from references 4 and 6 and with unpublished data from the Ames 6- by 6-foot and 8- by 7-foot wind tunnels. The data from five facilities are in good agreement. Included in the figure are values of C_{m_α} computed from modified Newtonian impact theory. Comparison of the calculated values with the data from the present tests near a Mach number of 4 shows that the modified theory closely predicts the moment-curve slope of both body shapes.

Drag

Coefficients of drag were determined from the deceleration of the models by the procedure described in reference 10. These drag data are represented by the circle symbols in figure 8 and are compared with data from reference 6 and unpublished data from the Ames 6- by 6-foot and 8- by 7-foot wind tunnels. The data from the various facilities are in good agreement. Included in the figure are values of C_D computed from modified Newtonian impact theory. Comparison of the calculated values with the data from the present tests shows that the modified theory underestimates the drag of the paraboloid by about 15 percent and overestimates the drag of the flat-faced model by about 10 percent.

CONCLUDING REMARKS

Results of the measurements at a Mach number of 4 of the stability and drag characteristics of two blunt-nosed, low-fineness-ratio bodies of revolution, one relatively flat-faced and the other a paraboloid, oscillating in free flight can be summarized as follows.

The dynamic stability of both body shapes was found to be a function of angle of attack. The flat-faced model was dynamically unstable throughout the amplitude range from 4° to 16°. The greatest instability occurred near 8° amplitude. The parabolic model was dynamically stable throughout most of the amplitude range of the tests. This body was unstable at the lowest amplitude tested, 4°, and neutrally stable at the highest amplitude, 27°. Modified Newtonian impact theory does not predict a variation of dynamic stability with angle of attack, whereas, a variation is shown by the data of the present tests. Values of the damping-in-pitch derivative, $C_{m_q} + C_{m_{\dot{\alpha}}}$, were found to be stabilizing throughout most of the test range. The divergence in oscillation of the flat-faced model was thus attributable to the high drag coefficient and negative lift-curve slope.

The static stabili of both the parabolic and the flat-faced models as measured in five facilities at the Ames Research Center over a wide Mach number range form a consistent set of data. Modified Newtonian impact theory closely predicts the moment-curve slope of both body shapes near a Mach number of 4.

The drag data from the present tests and the data from wind-tunnel tests are in good agreement. Modified Newtonian impact theory underestimates the measured drag of the paraboloid by about 15 percent and overestimates the measured drag of the flat-faced model by about 10 percent near a Mach number of 4.

Ames Research Center
National Aeronautics and Space Administration
Moffett Field, Calif., Mar. 11, 1959

[redacted]

[redacted]

REFERENCES

1. Friedrich, Hans R., and Dore, Frank J.: The Dynamic Motion of a Missile Descending Through the Atmosphere. Jour. Aero. Sci., vol. 22, no. 9, Sept. 1955, pp. 628-632.

2. Allen, H. Julian: Motion of a Ballistic Missile Angularly Misaligned With the Flight Path Upon Entering the Atmosphere, and Its Effect Upon Aerodynamic Heating, Aerodynamic Loads, and Miss Distance. NACA TN 4048, 1957.

3. Sommer, Simon C., and Tobak, Murray: Study of the Oscillatory Motion of Manned Vehicles Entering the Earth's Atmosphere. NASA MEMO 3-2-59A, 1959.

4. DeRose, Charles E.: Normal-Force and Pitching-Moment Characteristics for Two Blunt-Nosed Re-entry Type Bodies From M = 2.4 to M = 4.0. NASA MEMO 2-4-59A, 1959.

5. Bird, John D., and Reese, David E., Jr.: Stability of Ballistic Reentry Bodies. NACA RM L58E02a, 1958.

6. Buell, Donald A., and Johnson, Norman S.: An Experimental Investigation of the Dynamics of Two Blunt Bodies at Subsonic Speeds. NASA TM X-18, 1959.

7. Seiff, Alvin, Sommer, Simon C., and Canning, Thomas N.: Some Experiments at High Supersonic Speeds on the Aerodynamic and Boundary-Layer Transition Characteristics of High-Drag Bodies of Revolution. NACA RM A56I05, 1957.

8. Nicolaides, John D.: On the Free Flight Motion of Missiles Having Slight Configurational Asymmetries. B.R.L. Rep. 858, Aberdeen Proving Ground, 1953.

9. Shinbrot, Marvin: A Least Squares Curve Fitting Method With Applications to the Calculation of Stability Coefficients From Transient-Response Data. NACA TN 2341, 1951.

10. Seiff, Alvin: A New Method for Computing Drag Coefficients from Ballistic Range Data. Jour. Aero. Sci., vol. 25, no. 2, Feb. 1958, pp. 133-134.

[redacted]

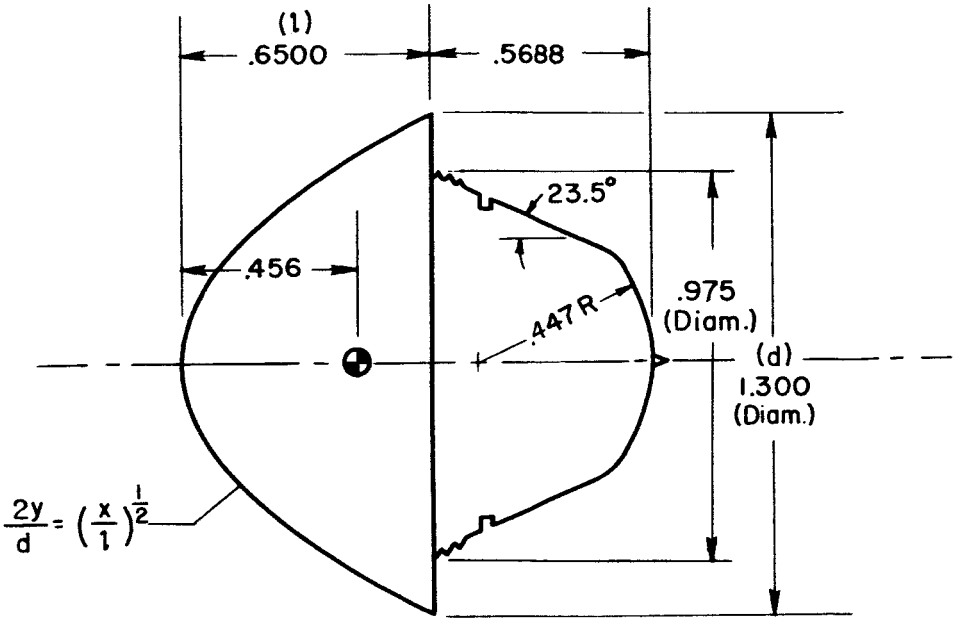

(a) Model with parabolic forebody, $(d/\sigma)^2$ = 13.8, weight = 47.7 grams.

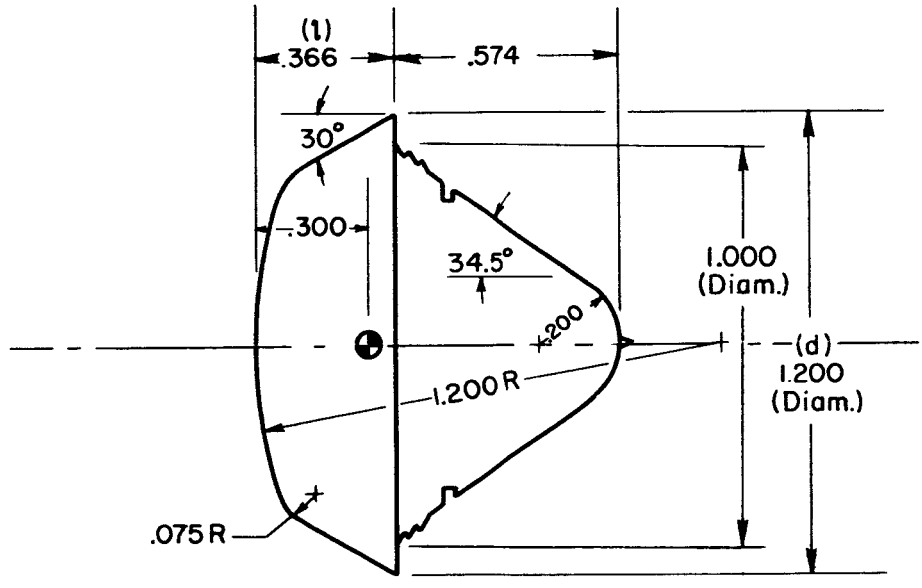

(b) Model with nearly flat front face, $(d/\sigma)^2$ = 17.1, weight = 44.6 grams.

Figure 1.- Sketches of models; all dimensions in inches.

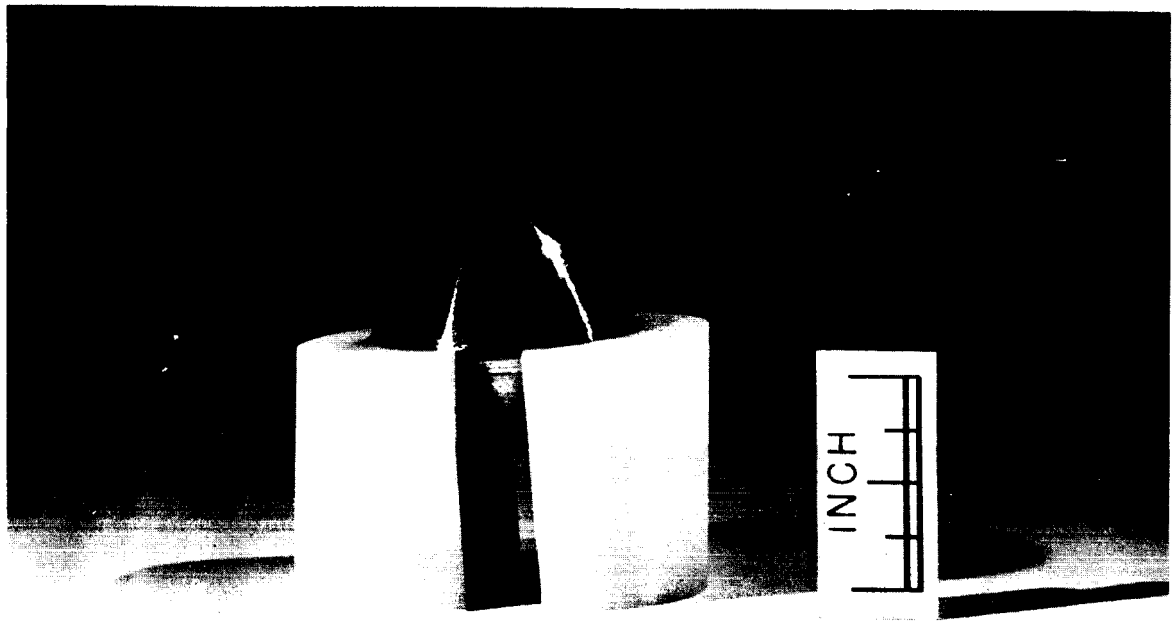

A-24557

Figure 2.- Photograph of sabot with parabolic model.

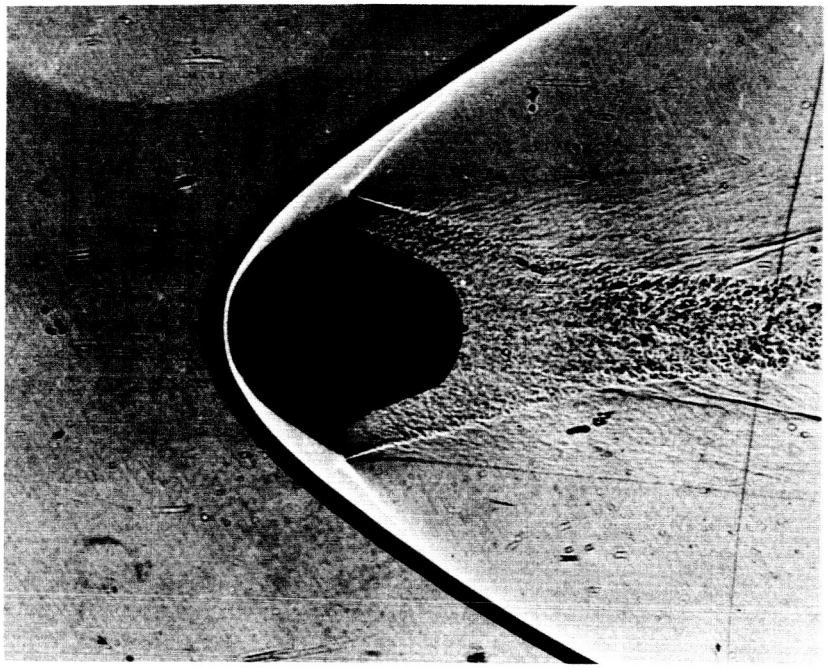

(a) Parabolic model, M = 3.6.

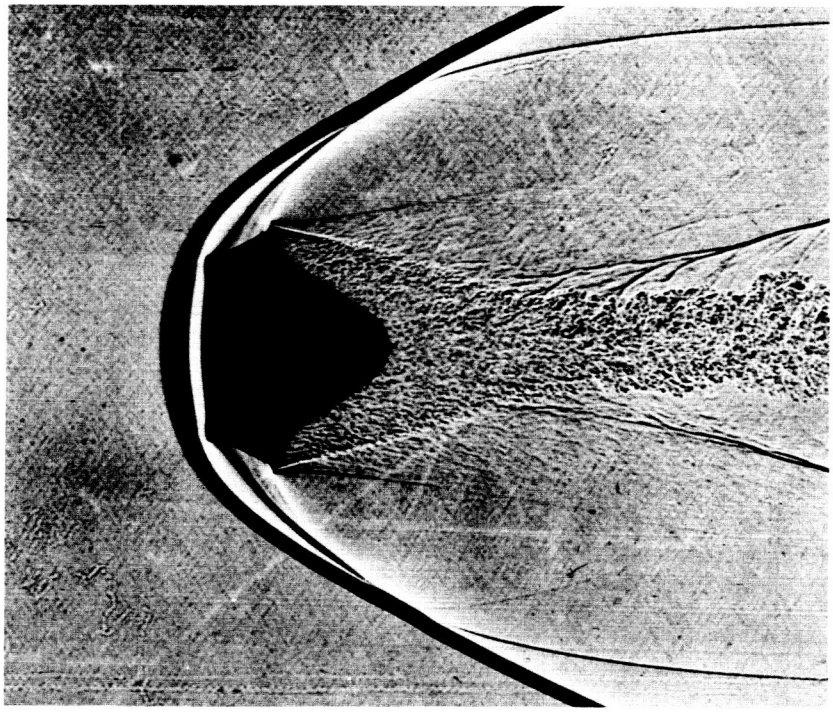

(b) Flat-faced model, M = 4.2.

A-24845

Figure 3.- Representative shadowgraphs.

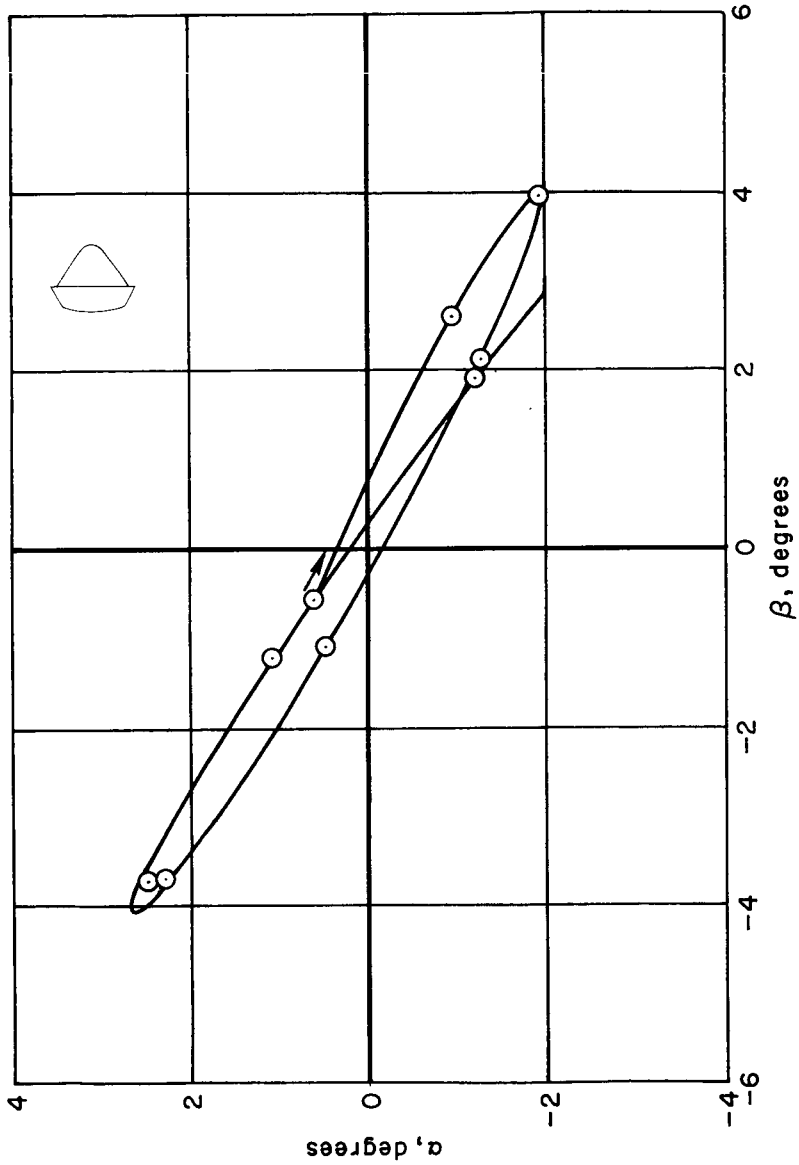

(a) Flat-faced model, peak amplitude 4.5°.

Figure 4.- Pitching and yawing motions.

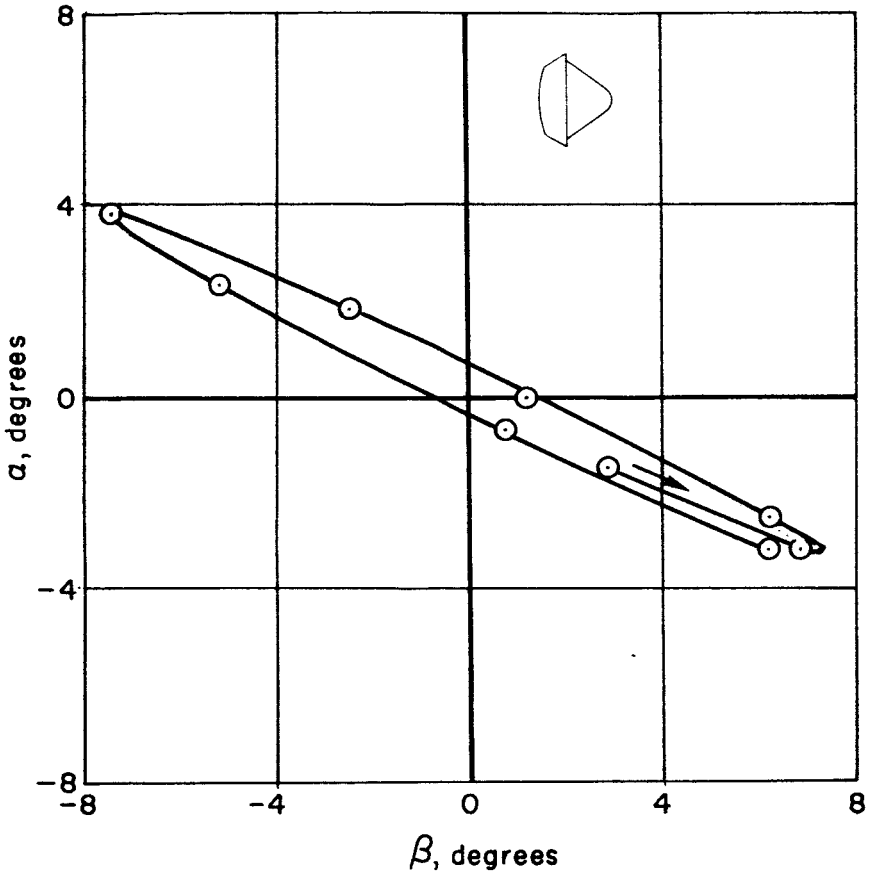

(b) Flat-faced model, peak amplitude 8.0°.

Figure 4.- Continued.

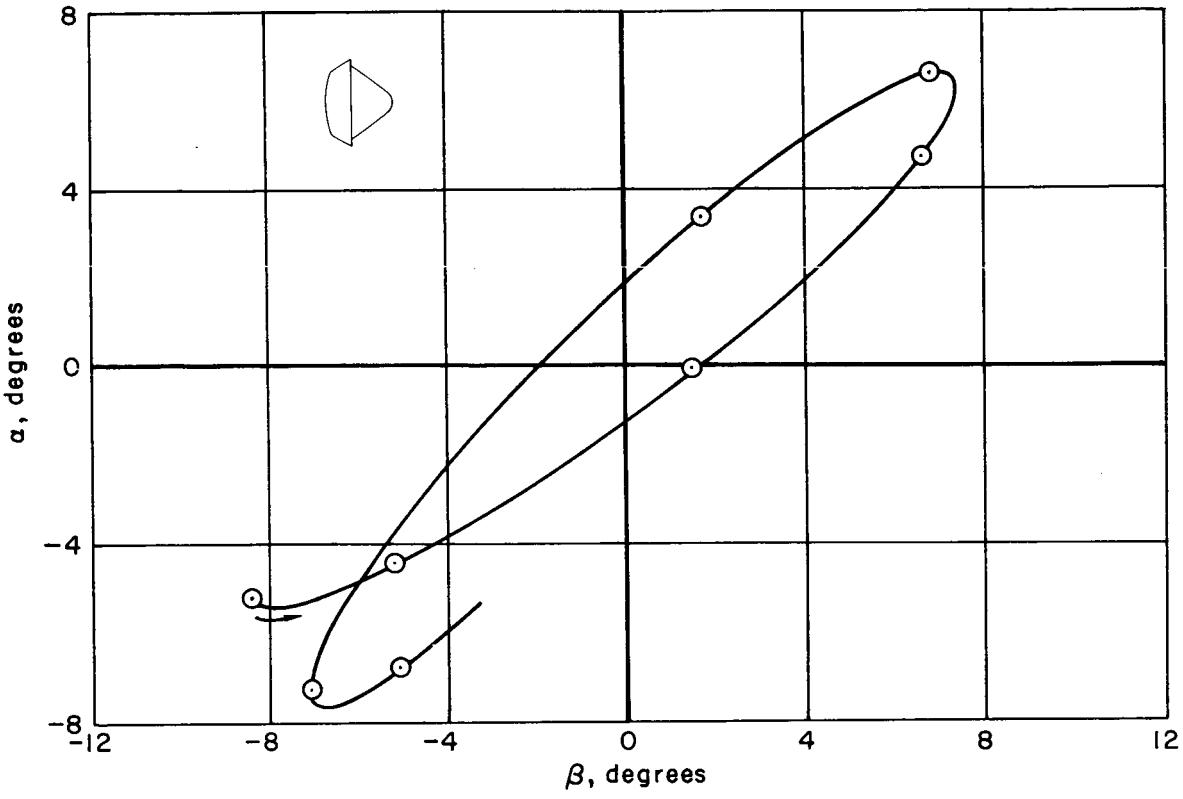

(c) Flat-faced model, peak amplitude 9.7°.

Figure 4.- Continued.

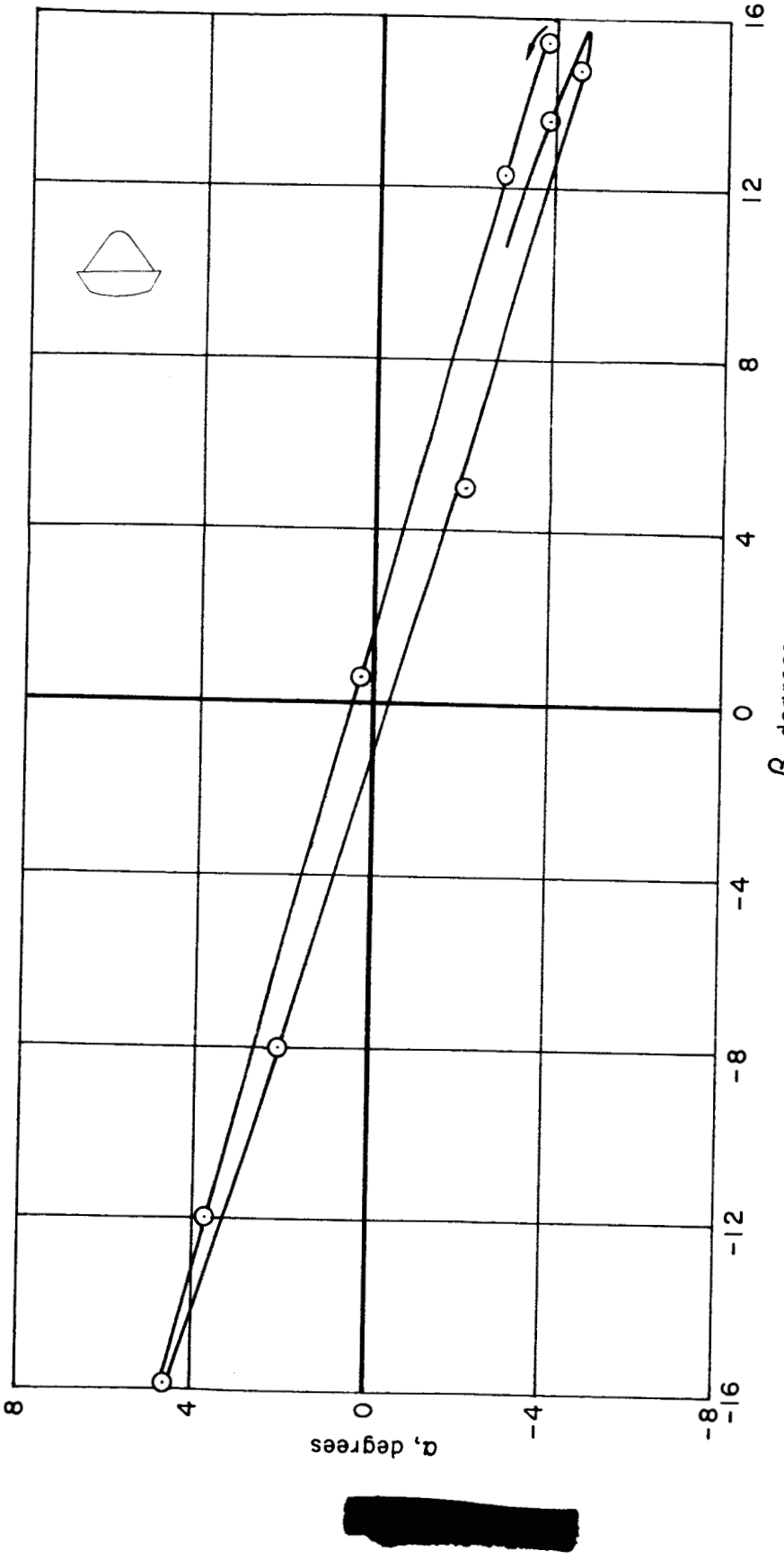

(d) Flat-faced model, peak amplitude 16.3°.

Figure 4.- Continued.

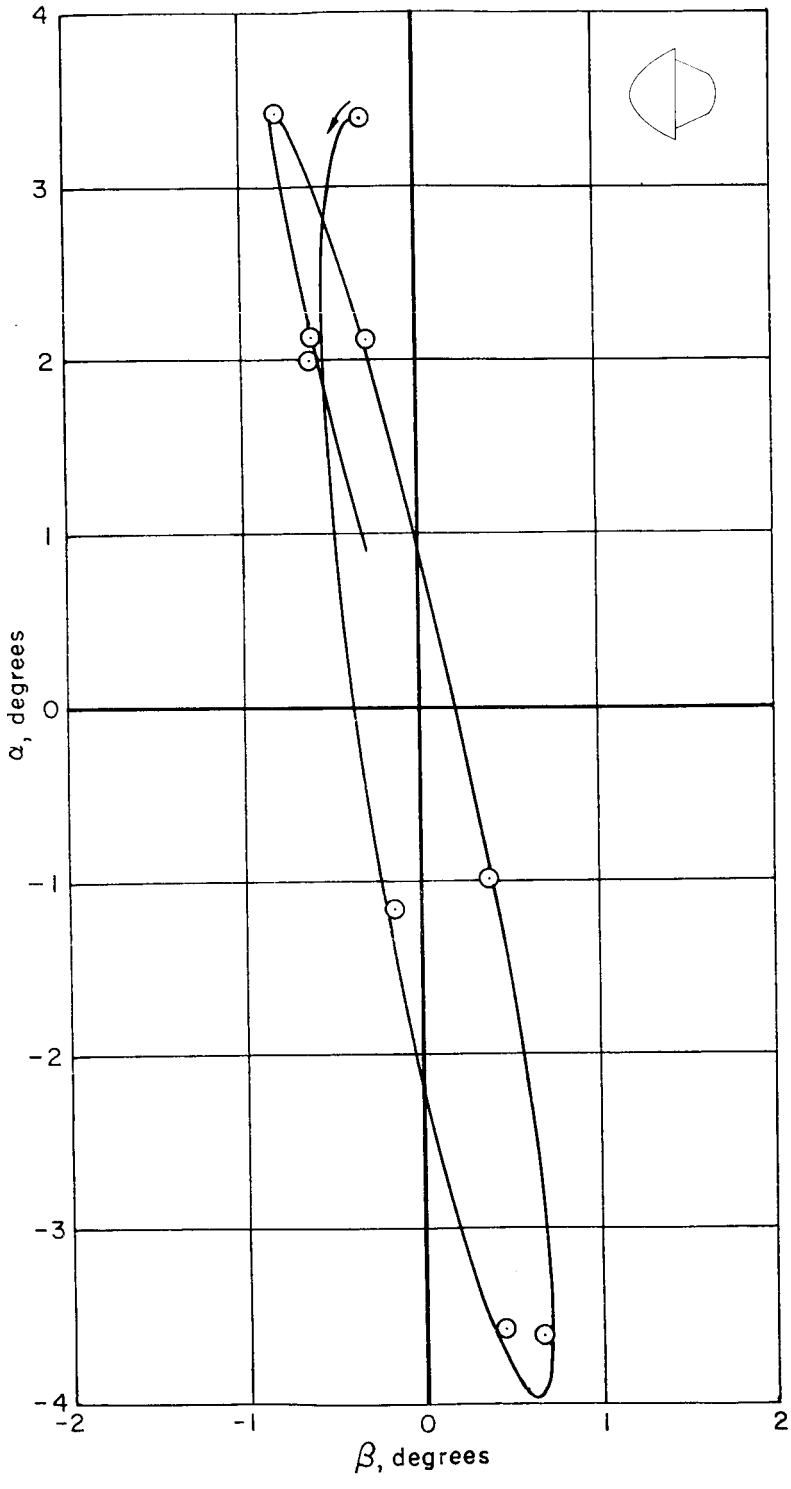

(e) Parabolic model, peak amplitude 3.8°.

Figure 4.- Continued.

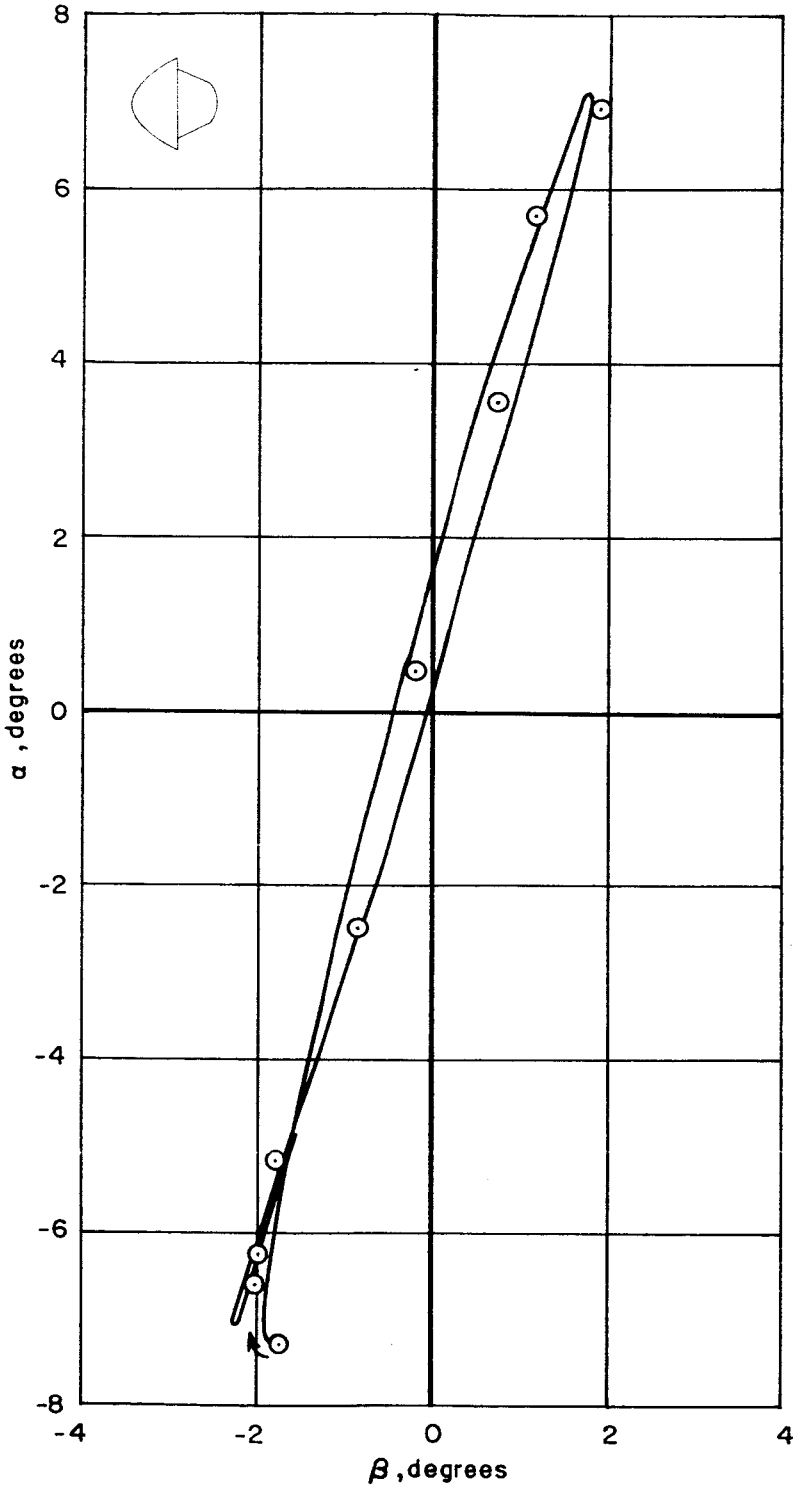

(f) Parabolic model, peak amplitude 7.5°.

Figure 4.- Continued.

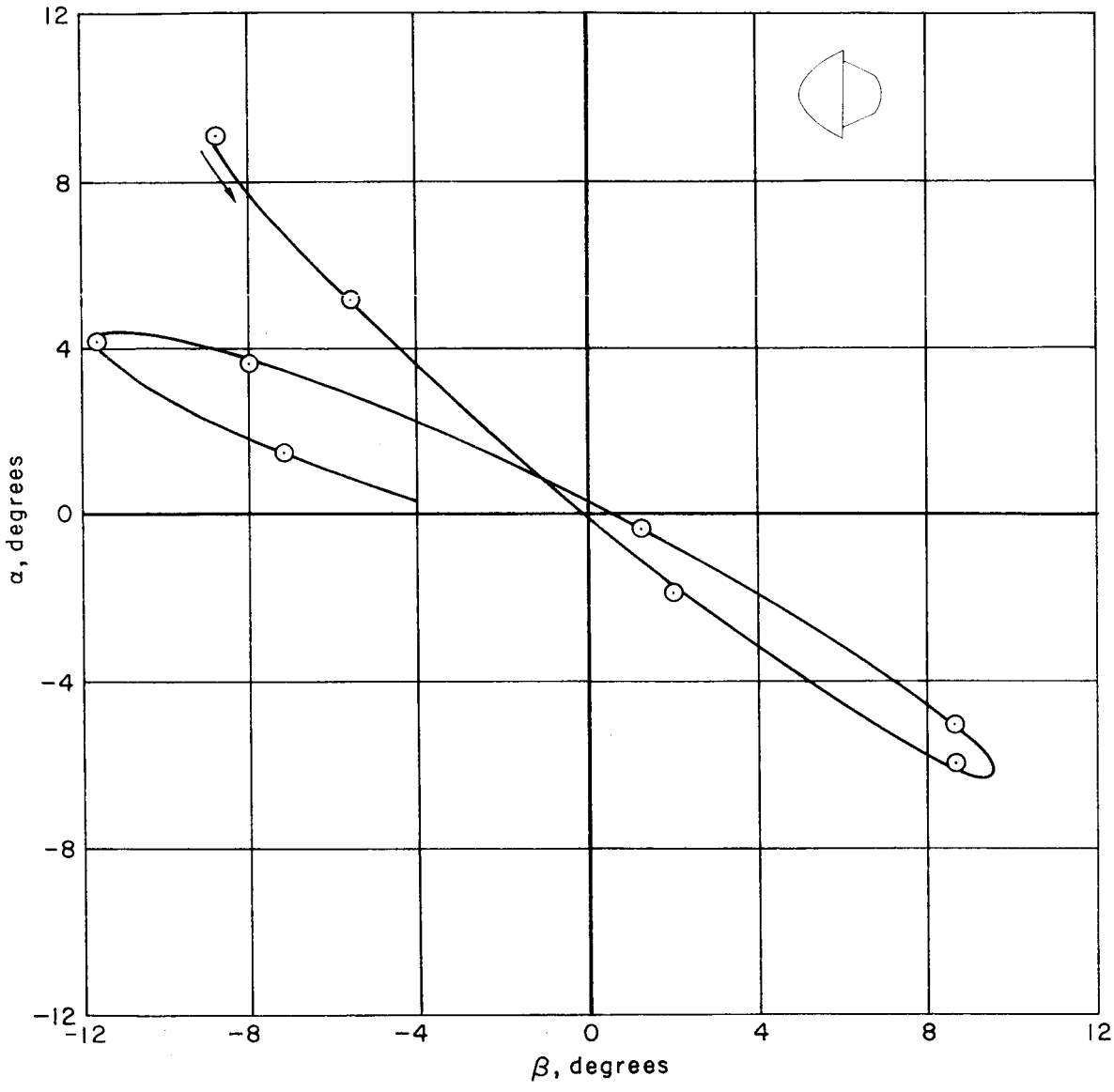

(g) Parabolic model, peak amplitude 11.7°.

Figure 4.- Continued.

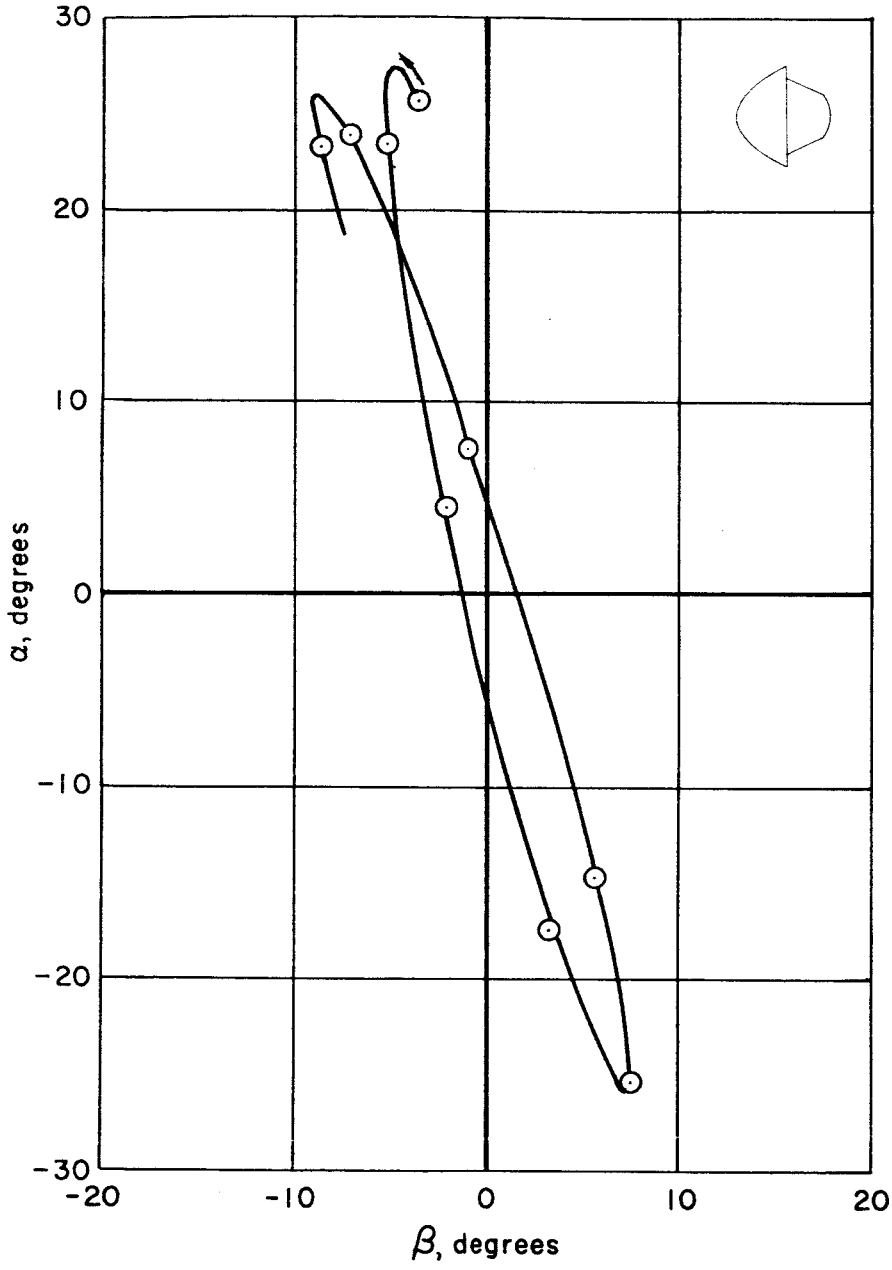

(h) Parabolic model, peak amplitude 27.2°.

Figure 4.- Continued.

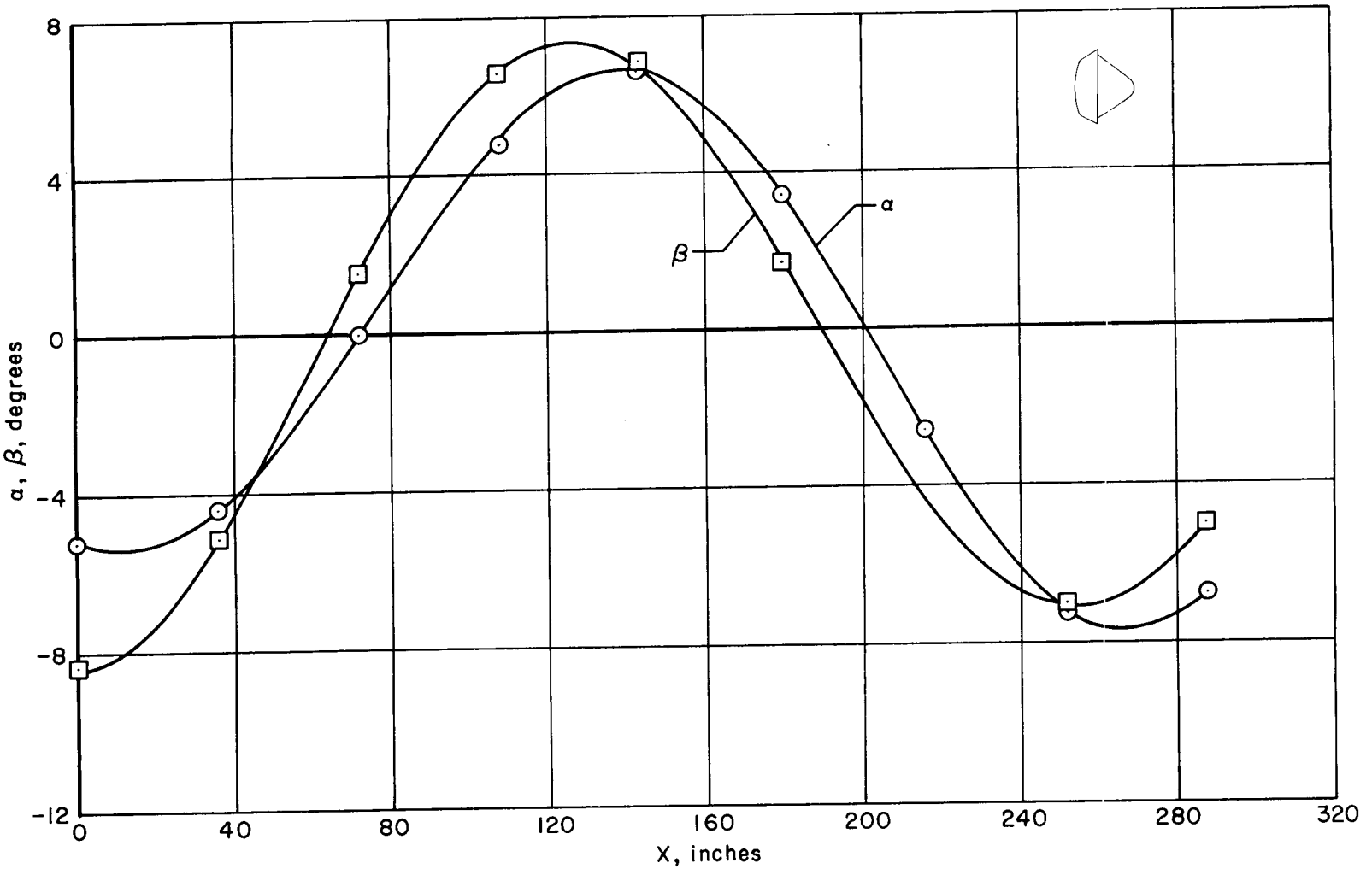

(i) Angle-distance history of flat-faced model (α-β plane in fig. 4(c)).

Figure 4.- Continued.

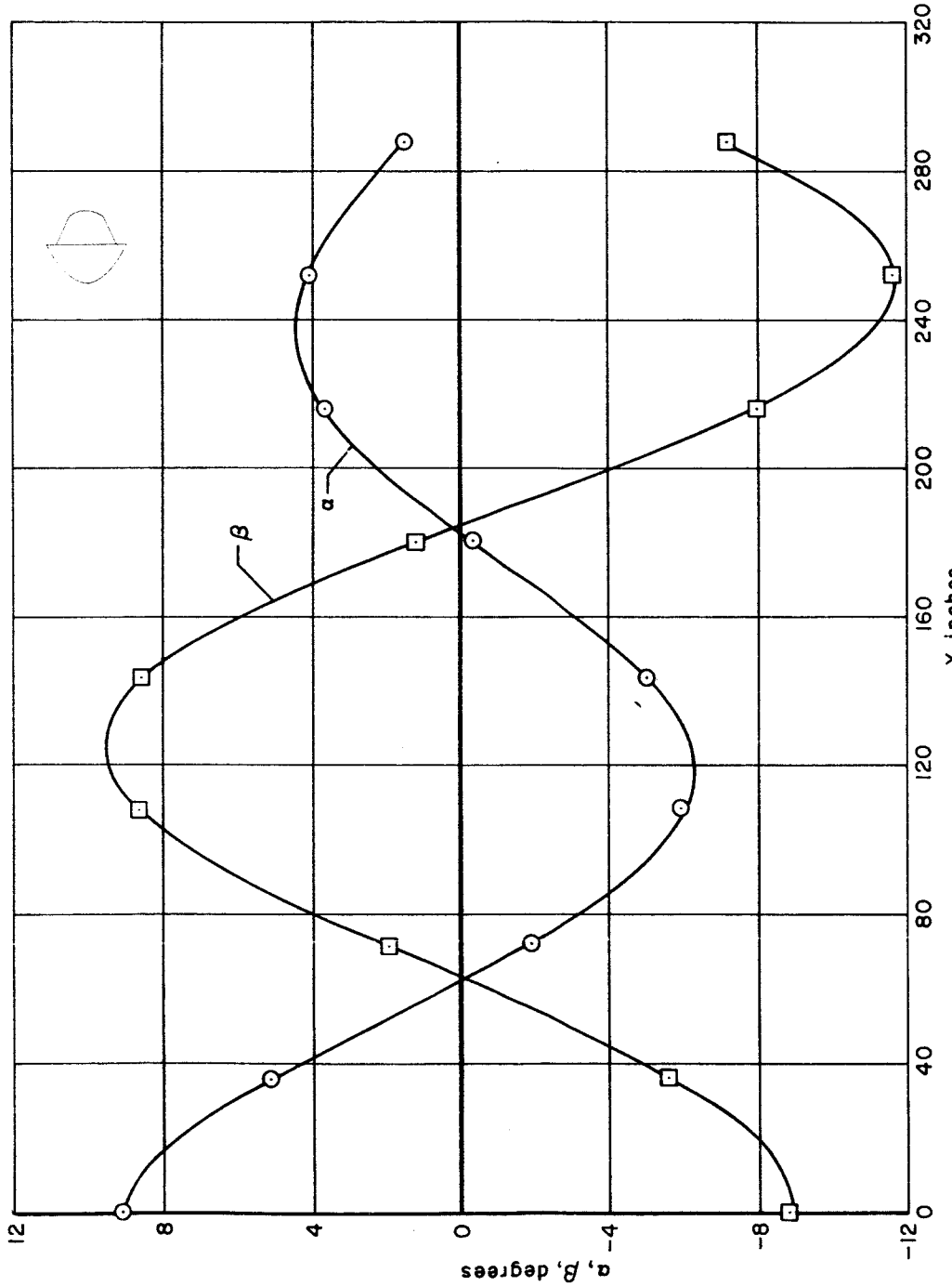

(j) Angle-distance history of parabolic model (α-β plane in fig. 4(g)).

Figure 4.- Concluded.

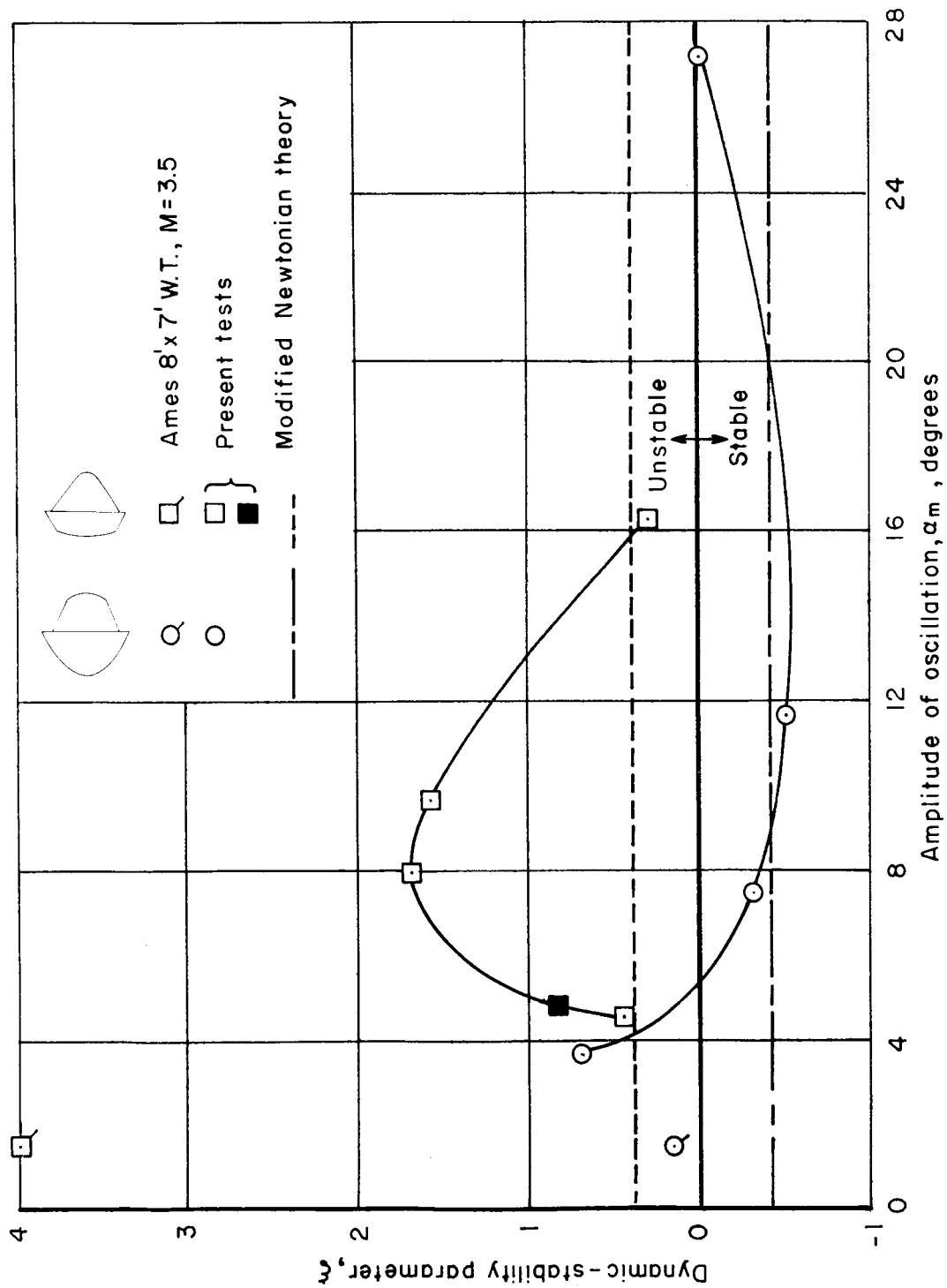

Figure 5.- Dynamic-stability data.

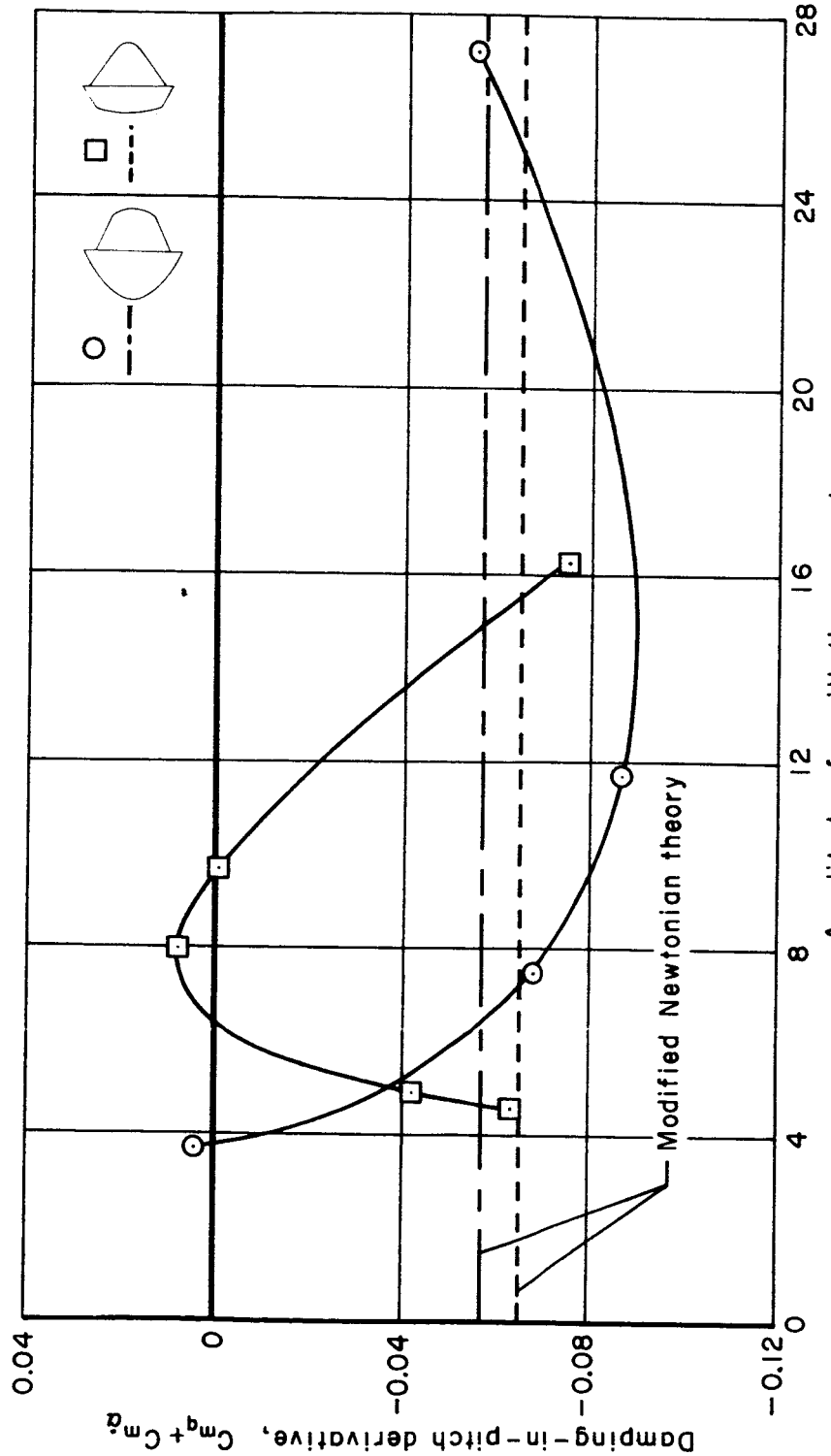

Figure 6.- Damping-in-pitch derivative.

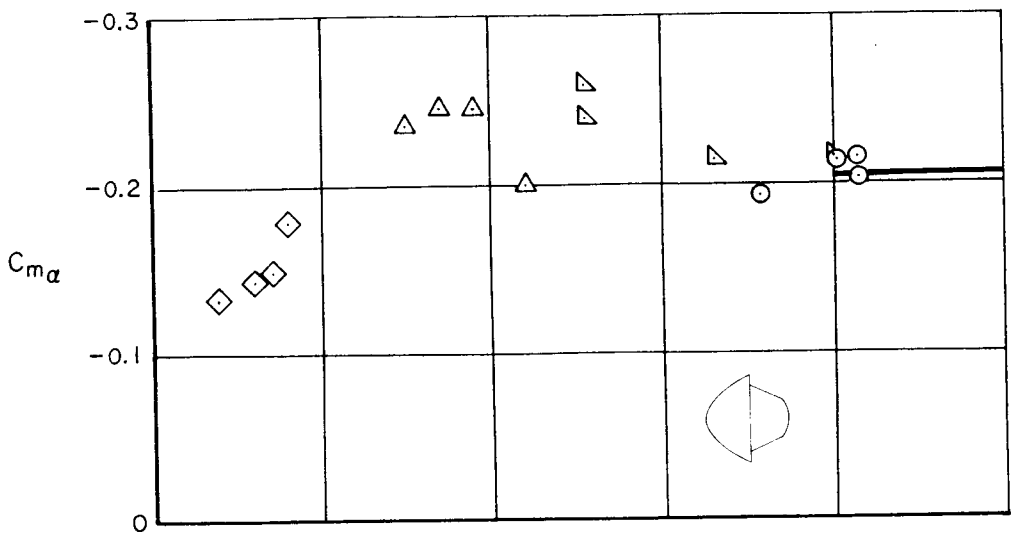

(a) Parabolic model.

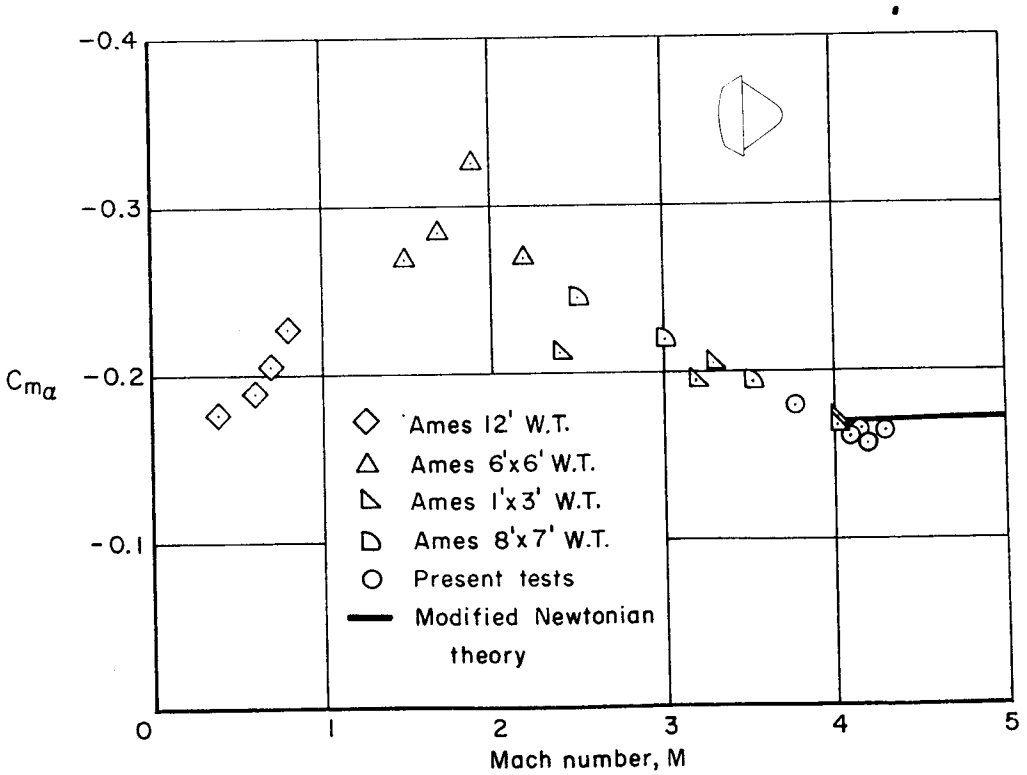

(b) Flat-faced model.

Figure 7.- Static-stability data.

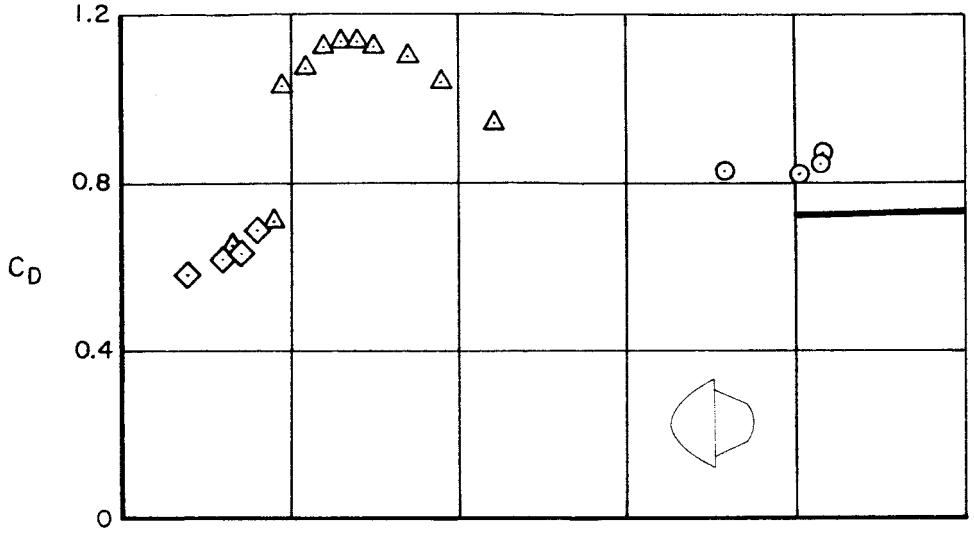

(a) Parabolic model.

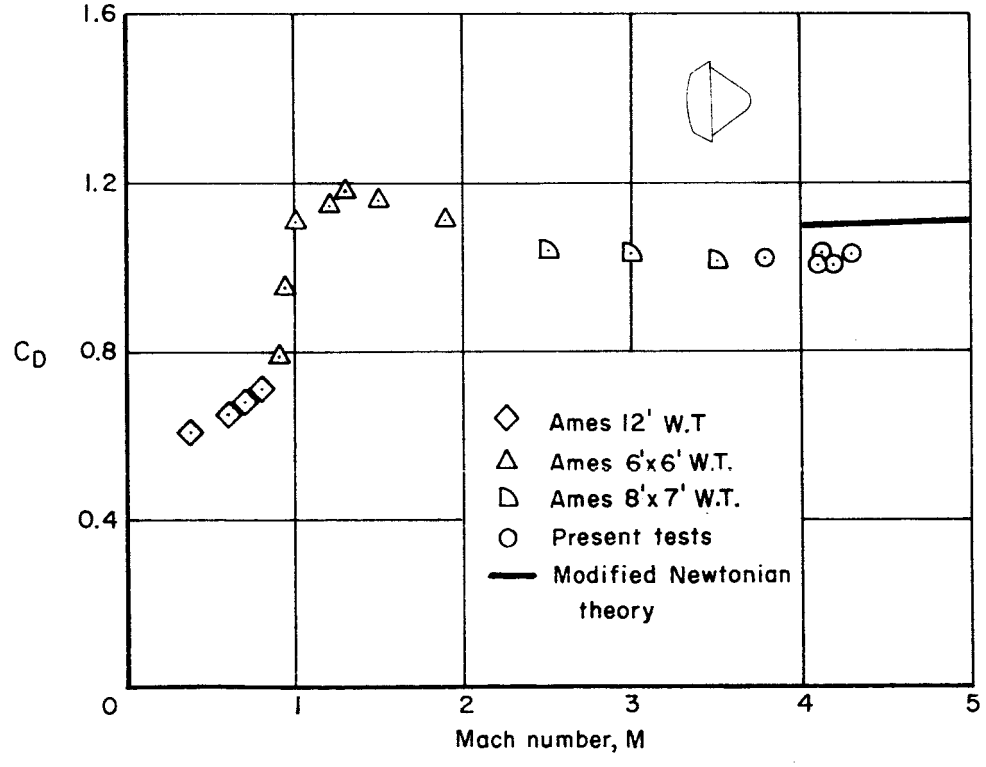

(b) Flat-faced model.

Figure 8.- Drag data.